World of Science: Journal on
Modern Research Methodologies

Volume 2 Issue 12, Year 2023
ISSN: 2835-3072
https://univerpubl.com/index.php/woscience

Green Synthesis of ZnO/Ag Nanoparticles and Their Effect on the Skin Determined Using IR Thermography

Alrabab Ali Zain Alaabedin, Basaad Hadi Hamza, Aseel Musafa Abdual-Majeed
Department of Physics, College of Science, Mustansiriyah University, Baghdad, Iraq

Article Information

Received: Oct 01, 2023
Accepted: Nov 02, 2023
Published: Dec 11, 2023

Keywords: *Green Synthesis; ZnO/Ag NPs; IR thermography*

ABSTRACT

In this study, a green synthesis approach was used to prepare (ZnO/Ag NPs). These Zno/Ag NPs' optical and structural characteristics were investigated using TEM, FE-SEM, X-ray diffraction, and UV-vis spectroscopy. The highest peak in the UV-vis absorption spectra was seen at 400 nm. The ZnO/Ag NPs that were created featured narrow, strong peaks that indicated high crystallinity of the nanoparticle. The X-ray pattern reveals that these peaks match to the ZnO hexagonal wurtzite phase structure. ZnO/Ag nanoparticles were spherical in shape, small (varying in size from 17.8 to 73.6 nm), and had regular, homogenous structures, according to the FE-SEM data. When ZnO/Ag NPs were investigated at various magnifications using TEM, it was discovered that they were primarily spherical and evenly distributed throughout the sample. Using infrared thermal imaging (IRT), it was possible to see how the skin's temperature changed when the ZnO/Ag NPs had an impact. Following that, the sample was applied to the skin in two different ways: first, by mixing it with water, and second, by applying Vaseline. Both applications included no radiation and produced a rise in temperature.It was determined how much the temperature change in two bands (3–5 and 8–14 µm) affected the radiance. For picture R8 without radiation, the highest value in the range (3-5) µm was (0.9733), while for image R2* with radiation, the highest value in the range (8–12) µm was (0.9365).As temperature rises, the total spectrum radioactive emission moves towards shorter wavelengths in proportion to the area under the curves. Radial heat diffusion is seen by comparing line profile data from various temperatures, which results in the energy from the submerged nanoparticles being transferred to the surrounding areas.

1. Introduction

Recently, nanoparticles have drawn a lot of attention because of their promise in many different fields [1,2]. Recently, there have been renewed expectations for both diagnosis and treatment due to the usage of nanoparticles in biological applications [3]. Research is now being conducted on the antibacterial and anticancer effects of this substance. Sadly, they are still in the early phases and require further in vivo and in vitro scientific investigation. Therefore, a wide range of unique physico-chemical properties and a wide range of prospective applications in the disciplines of material science and biological applications can be achieved by downsizing materials [4]. Zinc oxide (ZnO) has gained increased attention due to its numerous commercial applications, anticancer capabilities, and ability to function as a photocatalyst and antibacterial [5, 6]. Similar to ZnO, silver nanoparticles (AgNPs) are well known for their prospective applications in photocatalytic, antibacterial, and anticancer activities [7, 8]. The process of producing nanoparticles using biosynthesis is now more economical and reliable. One of the unique characteristics of nanoparticle biosynthesis is the selectivity of various nanoparticle morphologies depending on the biological source [9]. ZnO nanoparticles were prepared by Pillai et al. using extracts from four distinct plants (Beta vulgaris, Cinnamomum tamala, Cinnamomum verum, and Brassica oleracea var. Italica) and their antibacterial and antifungal characteristics were examined [10]. Ng et al. examined the Ag/ZnO combination and its potential to enhance photocatalytic degradation using Citrullus lanatus [11]. Noohpisheh et al. employed leaf extract from Trigonella foenum-graecum to produce ZnO/Ag nanocomposites. These composites were used to study their antimicrobial, antifungal, antioxidant, and photocatalytic activities [12]. Many different kinds of eco-friendly techniques for the synthesis of ZnO/Ag NPs have been documented [13]. Microorganisms or plant extract can be used in biological synthesis methods for nanoparticle manufacturing. The primary advantage is the potential employment of biologically generated nanoparticles in biological systems or directly in biological applications. Plant-mediated synthesis is one of the most attractive biological approaches due to its practicality, ease of use of readily available plants, and wide variety of morphologies. Plant extracts are utilised as capping and reducing agents in the green manufacture of nanoparticles because they include phenolic or polar components [14]. Citrus lemon, mentha piperita, and moringa oleifera, for instance, are excellent sources of flavonoids and phenolics [[15], [16], [17]. ZnO nanoparticles, or ZnO NPs, were recently created by Mousavi-Kouhi et al. via a green technique [18]. ZnO NPs were coated with silver to create Ag–ZnO nanocomposite (NCs). They showed that the Ag–ZnO NCs have antibacterial and anticancer qualities, which prevented the growth of cancerous and bacterial cells by acting as a cell toxin. Hosny et al. synthesised the ZnO/Ag Biohar nano-composite using a green synthesis approach [19]. They demonstrated the dual roles of Ag/ZnO@BC as a potent antibacterial agent against Klebsiella pneumonia and a promising antioxidant molecule. Saranya et al. chose to create ZnO/Ag nanocomposites using a green microwave-assisted technique [20]. According to their research, 39.58% of MCF-7 cells exhibited in vitro cytotoxicity when exposed to G-ZnO/Ag NCs. Similar to this, Beta vulgaris (beetroot) extract was used by Nagajyothi et al. to create ZnO/Ag nano-composites [21]. They showed that the ZnO/Ag 7.5 composite exhibited the strongest anticancer effects on the HeLa and SKOV-3 cell lines out of all the ZnO/Ag composites that were created.

In this study, the temperature shift and its impact on the skin were identified using the thermal imaging approach. This field's theoretical components must be briefly summarised in order to make the mechanism of action more understandable.

The spectral transmittance (τ_λ), which is the ratio of the spectral radiant power transmitted by the object, the spectral reflectance (ρ_λ), which is the ratio of the spectral radiant power reflected by the object, and the spectral absorbance (α_λ) are the three parameters employed in this study. These three parameters depend on the wavelength. At any wavelength, the total of these three parameters must equal one, as in Equation 1:

$$\alpha_\lambda + \rho_\lambda + \tau_\lambda = 1 \text{ …….. (1)}$$

The electromagnetic radiation that heated bodies emit is made up of discrete energy units, or quanta, the size of which depends on a fundamental physical constant (the Planck constant, h), rather than being released in a continuous stream. According to Planck's law, all objects emitted radiation over zero kelvin temperature at all times and all wavelengths. The following equation can be used to express an object's radiation in terms of Planck's law: [22]

$$R_\lambda(T) = \frac{2\pi hc^2}{\lambda^5}\frac{1}{e^{\frac{hc}{kT\lambda}}-1}. \text{ .... (2)}$$

Where, R= spectral radiant emittance ($\boldsymbol{W\ cm^{-2}}\mu^{-1)}$, h $= 6.62 \times 10^{-34} Js$, k = Boltzmann's Constant = 1.381 × 10^{-23} J/K , c=3 × 10^{8} m/s , λ=wavelerngth of emitted radiation and T=temperature in kelvin.

2. Experimental

This section examines the concrete actions that have been done in accordance with the proper temporal sequence for assessing the work:

2.1. Preparation of S. officinalis extract

After being cleaned of dust and other contaminants with distilled water, S. officinalis was cut into small pieces and allowed to dry for ten days under the shade. Using a household grinder, the dried leaves were crushed into a fine powder. Then, 20 g of S. officinalis powder was combined with 100 ml of deionized water and heated to 100 °C for 20 minutes while being stirred magnetically. After cooling to ambient temperature, the mixture was filtered and centrifuged for ten minutes at 3500 rpm. At that point, the extract might be used right away.

2.2. Green synthesis of (ZnO/Ag NPs) using S. officinalis extract

0.4g NaOH was dissolved in 50 ml of distilled water, placed in a beaker, and stirred over a stirrer until dissolved. Then 10 ml of silver nanoparticles prepared in advance was added to the beaker. $Zn(NO_3).6H_2O$ 1.89 is also placed in another beaker with 50 ml of distilled water and placed over a stirrer until completely dissolved. Then 10 ml of the plant extract was added to the NaOH, stirred until uniform, and added drop by drop to the mixture in the second beaker. The material was centrifuged and washed several times with water and ethanol. Finally, the material was dried at 30 °C on a stirrer.

2.3. Infrared (IR) imaging

After the ZnO/Ag NPs were prepared, they were placed on the skin of the rabbit. The Care and Use of Laboratory Animals Institute for Laboratory Animal Research Division's ARRIVE (Animal Research: Reporting of In Vivo Experiments) criteria were followed for all animal handling procedures. https://grants.nih.gov/grants/olaw/guide-for-the-care-and-use-of-laboratory-animals.pdf. Then IR camera using to take images.

The rabbit's feet were de-furmed, as depicted in Figure 1, and the material was applied to the skin in two different methods. In the first technique, 0.2 g of AgNPs were combined with 2 ml of distilled water, while in the second, 0.2 g of AgNPs were combined with 0.1 g of Vaseline.

After the material was applied to the skin, it was heated to a temperature of 2 cm using a nozzle that was 75 cm away from the skin. Images were taken every two minutes during this process. In both situations, high temperatures were noted.

Fig.1. A real picture of a rabbit

2.4. Characterization of ZnO/Ag NPs prepared from S. officinalis extract.

Using X-ray diffraction (XRD, SHIMADZU, CuKα radiation target: CU, current = 30 mA, voltage = 40 kV, $\lambda = 1.542$ Ao, scanning speed = 5 deg /min) with 2θ from 25° to 85°, the crystal structure and crystallinity of Ag NPs were examined.Using field emission scanning electron microscopy (FE-SEM, Hitachi S-4160), which has a continuous magnification power range of 6x to 100,000x, the morphology of the nanomaterial was examined. With FE-SEM, energy dispersive X-ray is employed. Tehran, Iran (TEM: ZEISS LEO 912 Ab, Germany). The absorption spectra of ZnO/Ag NPs that were synthesised were measured using a Lasany LI-2800 UV-visible spectrophotometer.

3. Results and Discussion

3.1. Structural analysis

X-ray diffraction analysis confirmed that ZnO/AgNPs were successfully synthesised. The narrow and powerful diffraction peaks of pure ZnO-NPs are shown in Figure (2), which suggests that the nanoparticle has a high degree of crystallinity. These peaks have two values of 31.76°, 34.42°, 36.25°, 47.56°, 56.60°, 62.86°, and 67°, and they correspond to the crystal planes (100), (002), (101), (102), (110), (103), and (112). Based on JCDPS Cardno. 89-1397 data, it is confirmed that these peaks match the phase structure of ZnO hexagonal wurtzite. No peaks were present that may be linked to any unidentified substances.

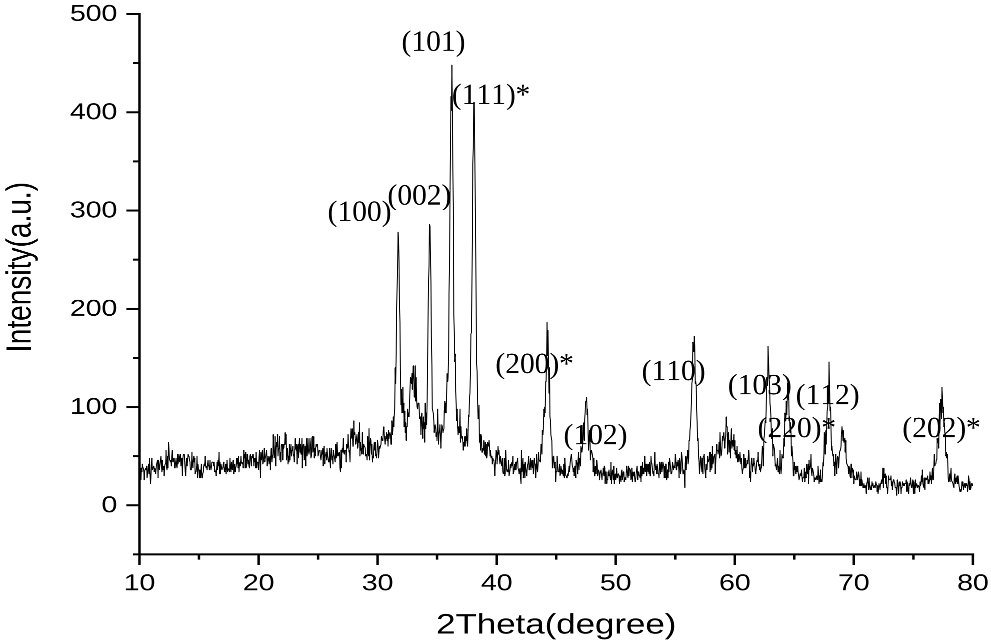

Fig. 2. XRD pattern of synthesized ZnO/Ag NPs.

Additionally, ZnO peaks were observed in the ZnO-Ag-NPs (fig. 4-3), demonstrating the successful formation of the crystalline structures. In a diffraction pattern, the two values for Ag's (111), (200), (220), and (202) crystal planes were 38.11°, 44.27°, 64.59°, and 78.92°, respectively. These peaks may be used as an index for silver in the face-centered cubic phase, as demonstrated by JCDPS Cardno. 001-1167. Another indication that ZnO-Ag-NPs were successfully synthesised with plant extracts is the absence of additional diffraction peaks. The occurrence of a distinct line broadening in the diffraction peaks confirmed the formation of nanometer-sized particles [23,24], indicating that ZnO/Ag core/shell NPs were successfully formed.

3.2. Energy dispersive X-ray (EDX) analysis

Element detection through Energy Dispersive X-Ray Spectroscopy (EDS) revealed the presence of zinc (Zn), oxygen (O), and silver (Ag) elements in the ZnO/Ag core/shell nanoparticles was confirmed by the EDX spectrum, in the sample (Figure 3). The composition of the core/shell NPs, as confirmed by the EDX analysis, was pure, with no other impurity elements present. The green synthesis successfully synthesized ZnO/Ag core/shell nanoparticles, as evidenced by the EDX spectra, confirming the verified XRD result. Using EDS, the relative amounts of Zn, O, and Ag were quantitatively determined to be 80 , 13.7, and 6.3%, respectively.

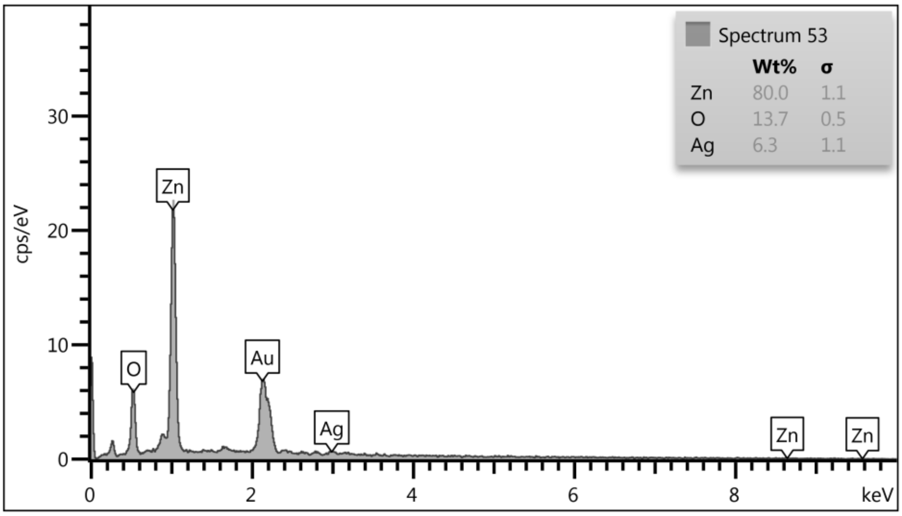

Fig.3.: Representing the percentage of metals inset is the atomic weight percentage of elements of the ZnO/Ag NPs.

3.3. Ultraviolet-visible (UV-Vis) spectroscopy analysis

The UV-vis spectroscopy was also used to confirm the NPs' production. The excitonic absorption peaks were red-shifted from 300 nm to 400 nm by the ZnO-Ag-NPs' localised surface plasmon resonance (LSPR), as shown in Figure (4). This shift in the band-gap energy indicates that the Ag atoms in the ZnO lattice were successfully changed by Ag+ ions substituting for Zn2+ atoms. Figure (4) shows the optical absorption of the ZnO/Ag core/shell NPs.

Furthermore, the green synthesis method—which uses an extract from S. officinalis—is thought to be very effective and environmentally benign. The chemical components that can be used in infrared thermography are reduced by the reducing agent that these plant extracts provide.

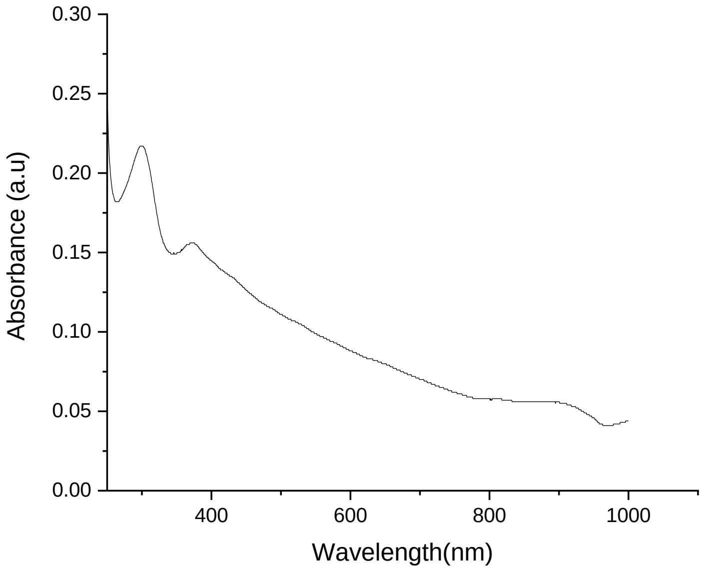

Fig.4. UV-visible absorption spectra of synthesized ZnO/Ag NPs

3.4. Field emission scanning electron microscopy (FE-SEM)

Field emission electron microscopy (FESEM) was used to analyse the size and shape of the generated ZnO/Ag, as shown in Figurses. (4-6), which display FESEM images of ZnO/Ag nanoparticles synthesised by the green synthesis process at several magnifications. The FE-SEM images demonstrated that the created particles had a nanoparticle nature and morphology, that the nanoparticles agglomerated, and that complete separation was not achieved. The shapes of the ZnO/Ag core/shell NPs synthesized by the green synthesis had a spherical shape, were tiny (ranging in size from 17.8 to 73.6 nm), and had regular and homogeneous structures.

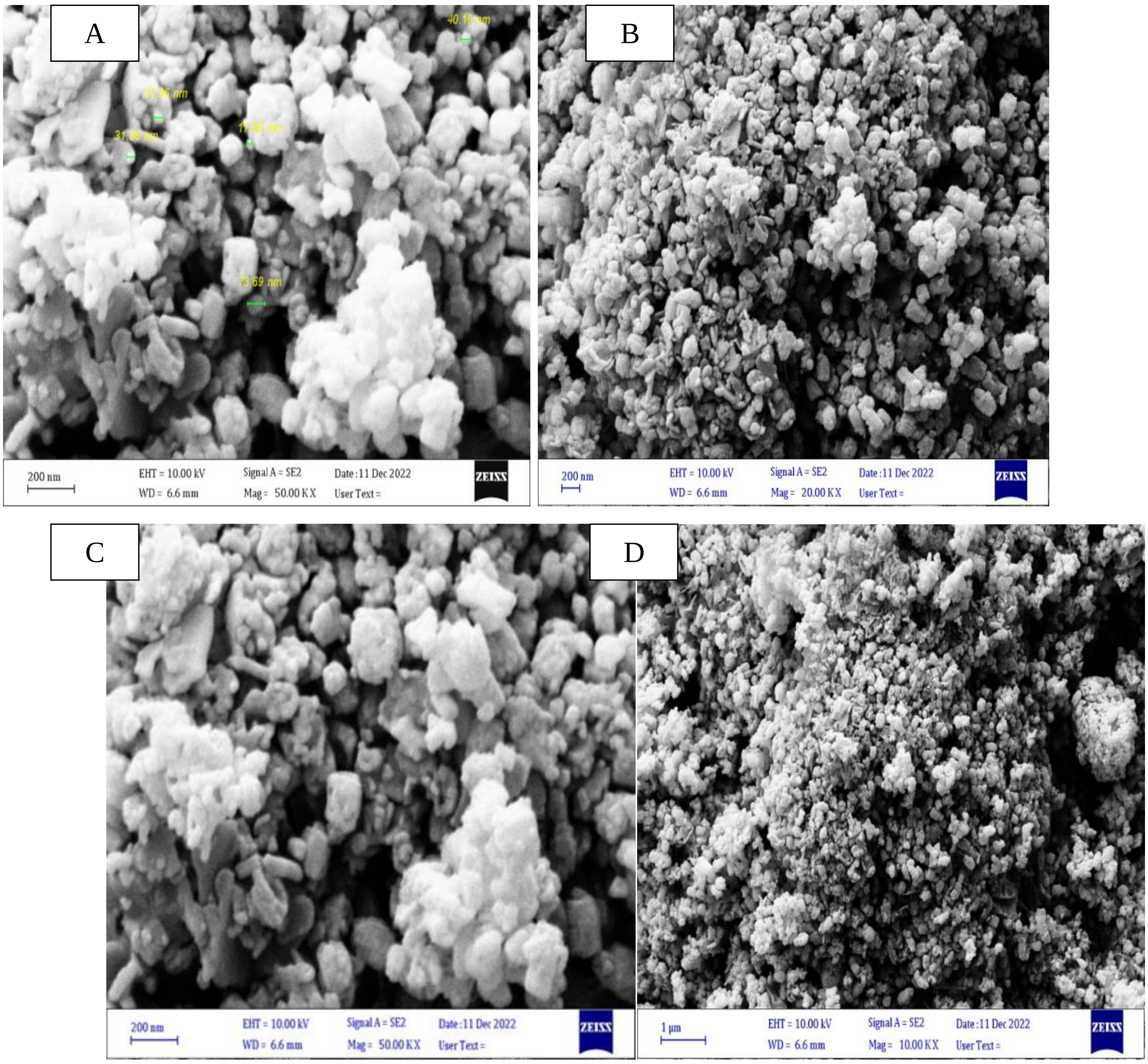

Figure (5) FE-SEM images of ZnO/Ag ,(A,B and C)with scale bar 200 nm,(D)with scale bar 1µm.

3.5. Transmission electron microscopy (TEM)

TEM images were used to analyse the nanoparticles' morphology and distribution (Figure 6). ZnO/Ag NPs were found to be mostly round and uniformly spread over the sample when analysed at different magnifications. A transmission electron microscopy (TEM) analysis was carried out to confirm the synthesis of the core/shell nanoparticles with green synthesis between the core and shells. The information relevant to the shape, size, and aggregation was also obtained from TEM analysis. Additionally, the TEM analysis demonstrated that there were two different regions. The dark inner part represented the core, and the shiny part surrounding the dark region represented the shell, confirming the synthesis of ZnO/Ag core/shell nanoparticles.

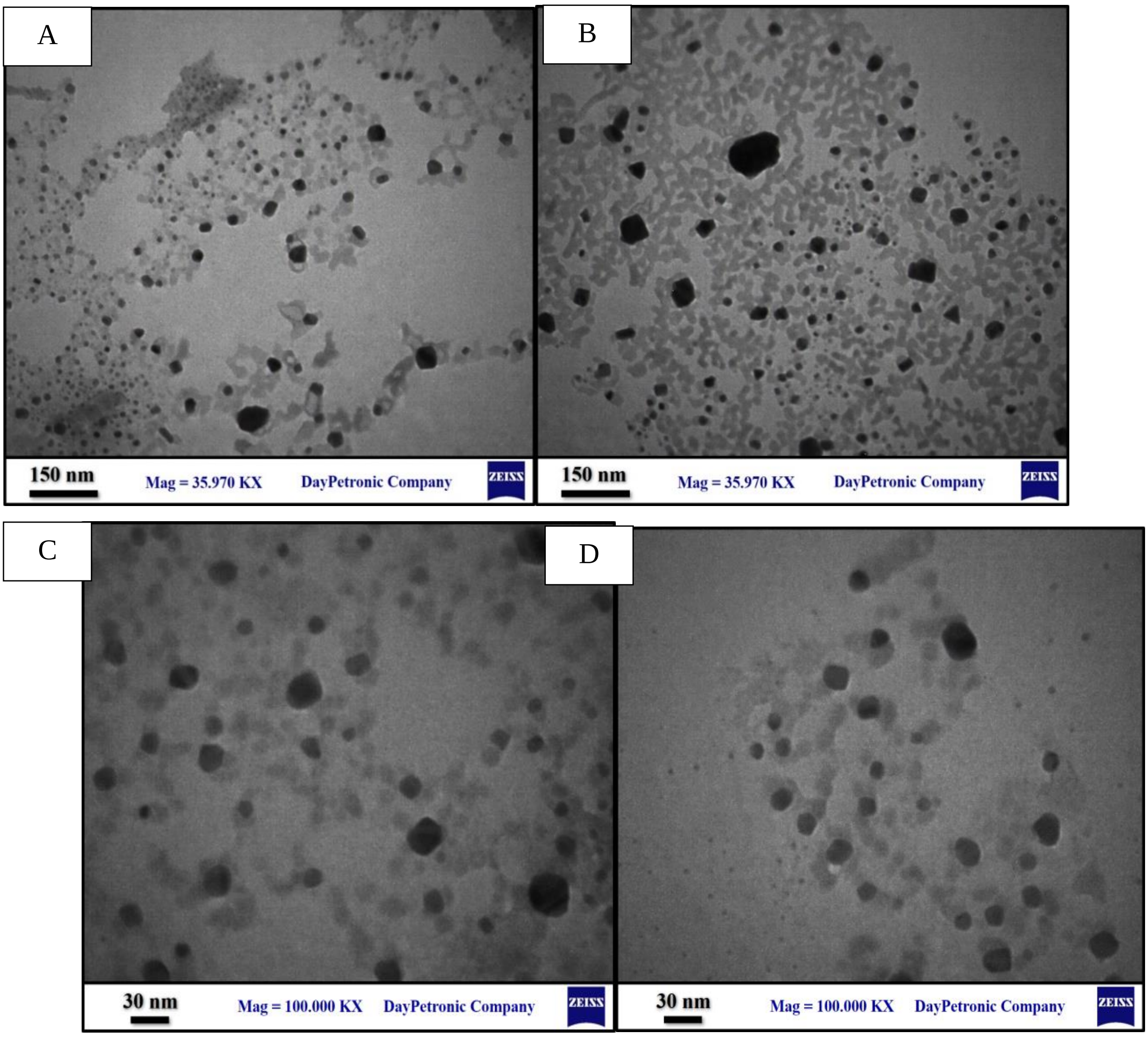

Figure(6). TEM images of ZnO/Ag NPs with an inset of different magnifications, (A,B)with scale bar 150 nm, (C,D)with scale bar 30 nm.

3.6. IR Thermography

IR thermography was performed used with a thermal camera (Ti10 Fluke). The thermal range of the image was 20.6 °C to 140.1 °C. The camera had a 20-mm lens, a thermal sensitivity (NETD) of ≤0.2 °C at 30 °C (200 mK), and an accuracy of ± 5 °C or 5 % (whichever is greater). The thermal photos were taken in the laboratories of the Department of Renewable Energy of the Ministry of Science and Technology (Baghdad, Iraq). These data show the temperature change and the effect of the ZnO/Ag NPs on the skin.

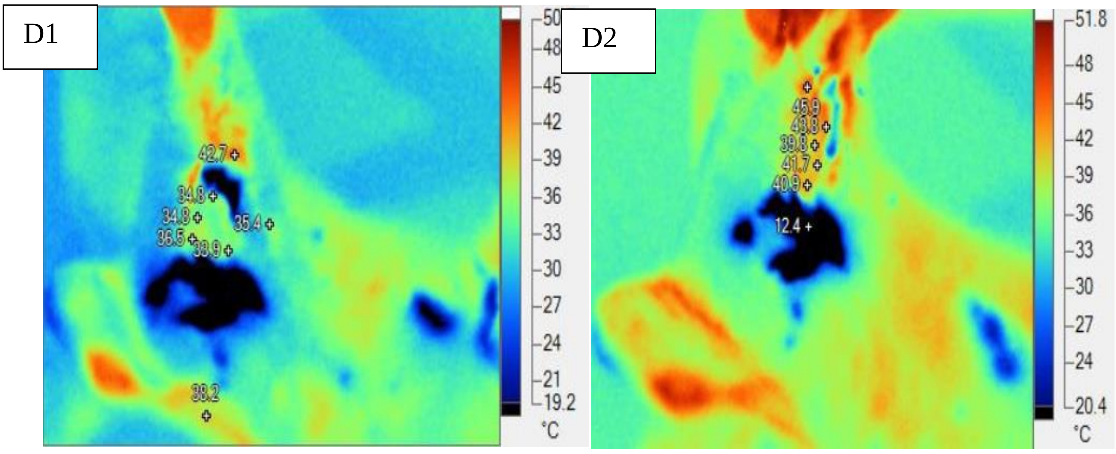

D3

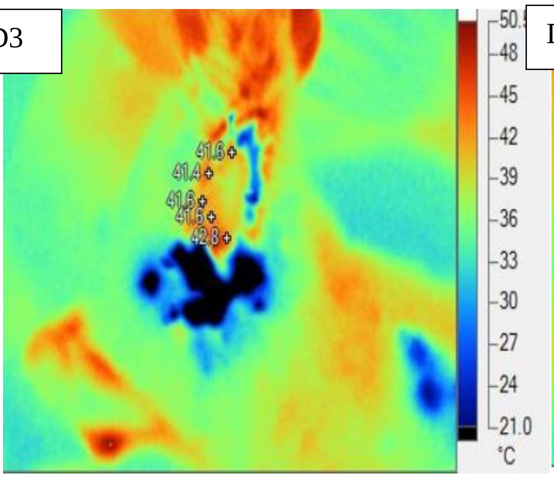

D4

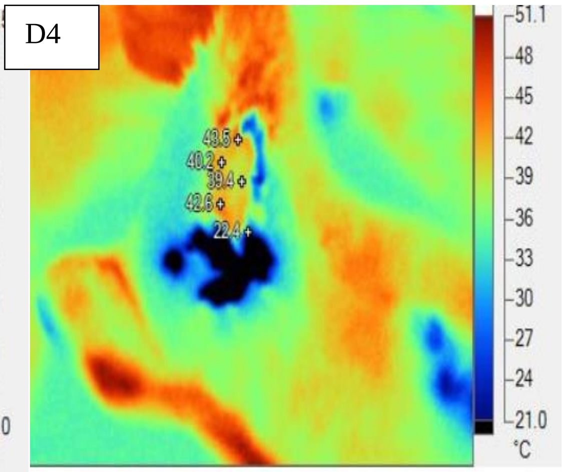

D5

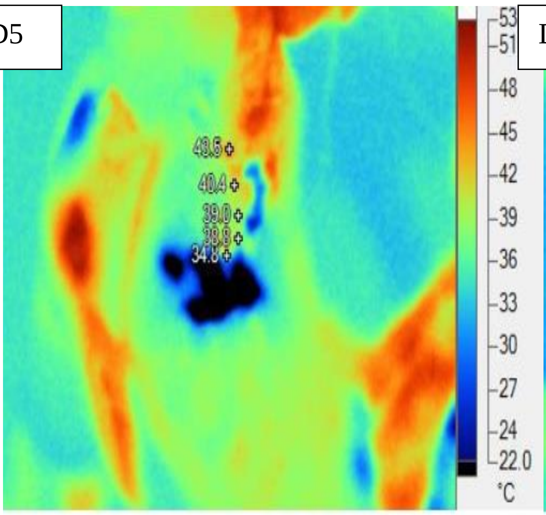

D6

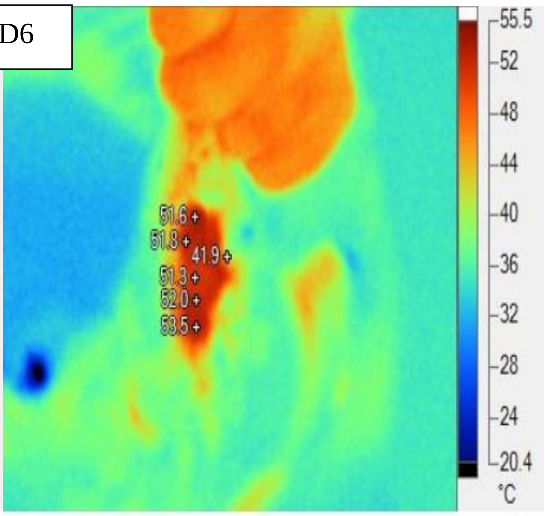

D7

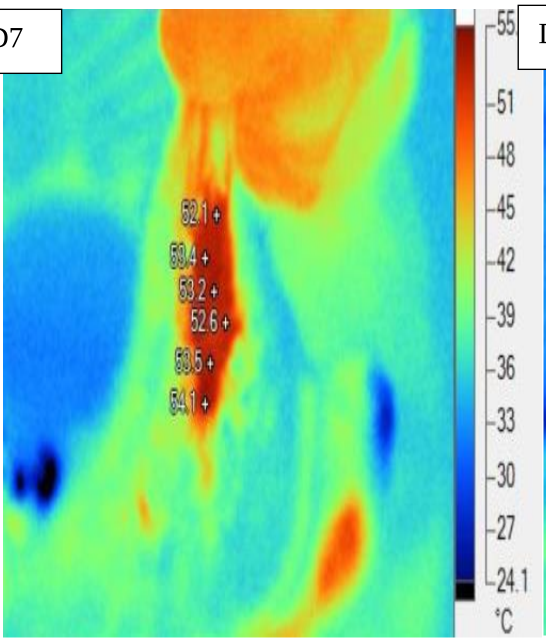

D8

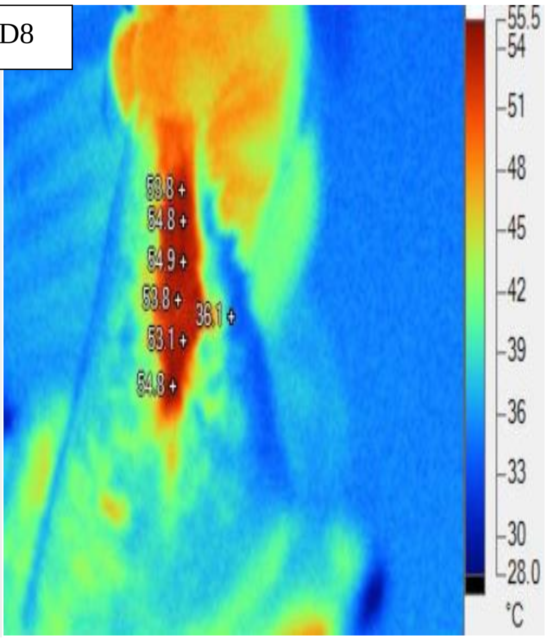

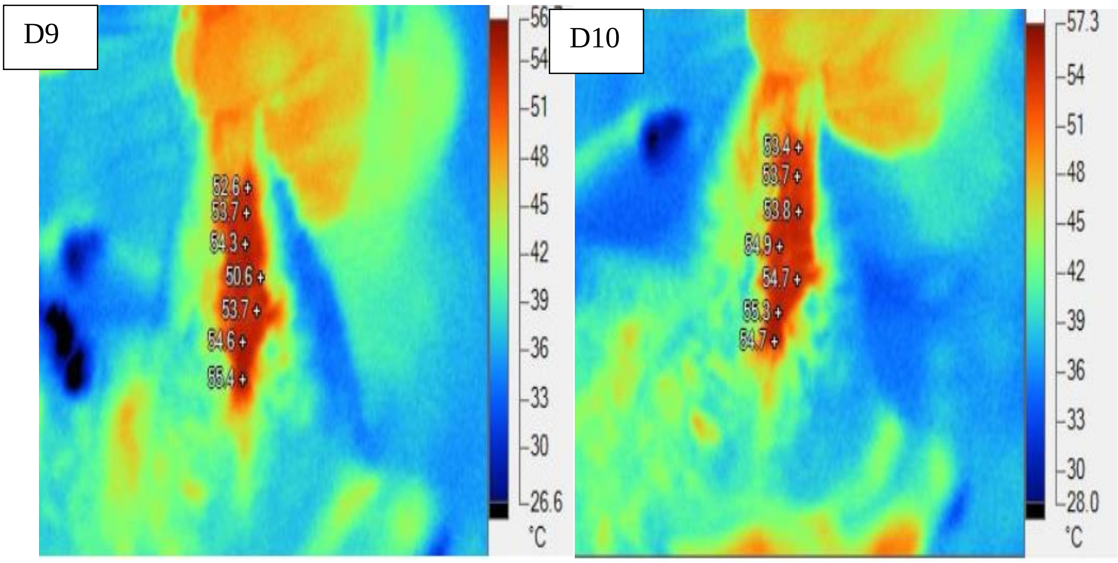

Fig.(7). Original photos taken without radiation for rabbit skin, (D1, D2, D3,D4,D5) mix ZnO/Ag NPs with water,(D6,D7,D8,D9,D10) mix ZnO/Ag NPs with Vaseline.

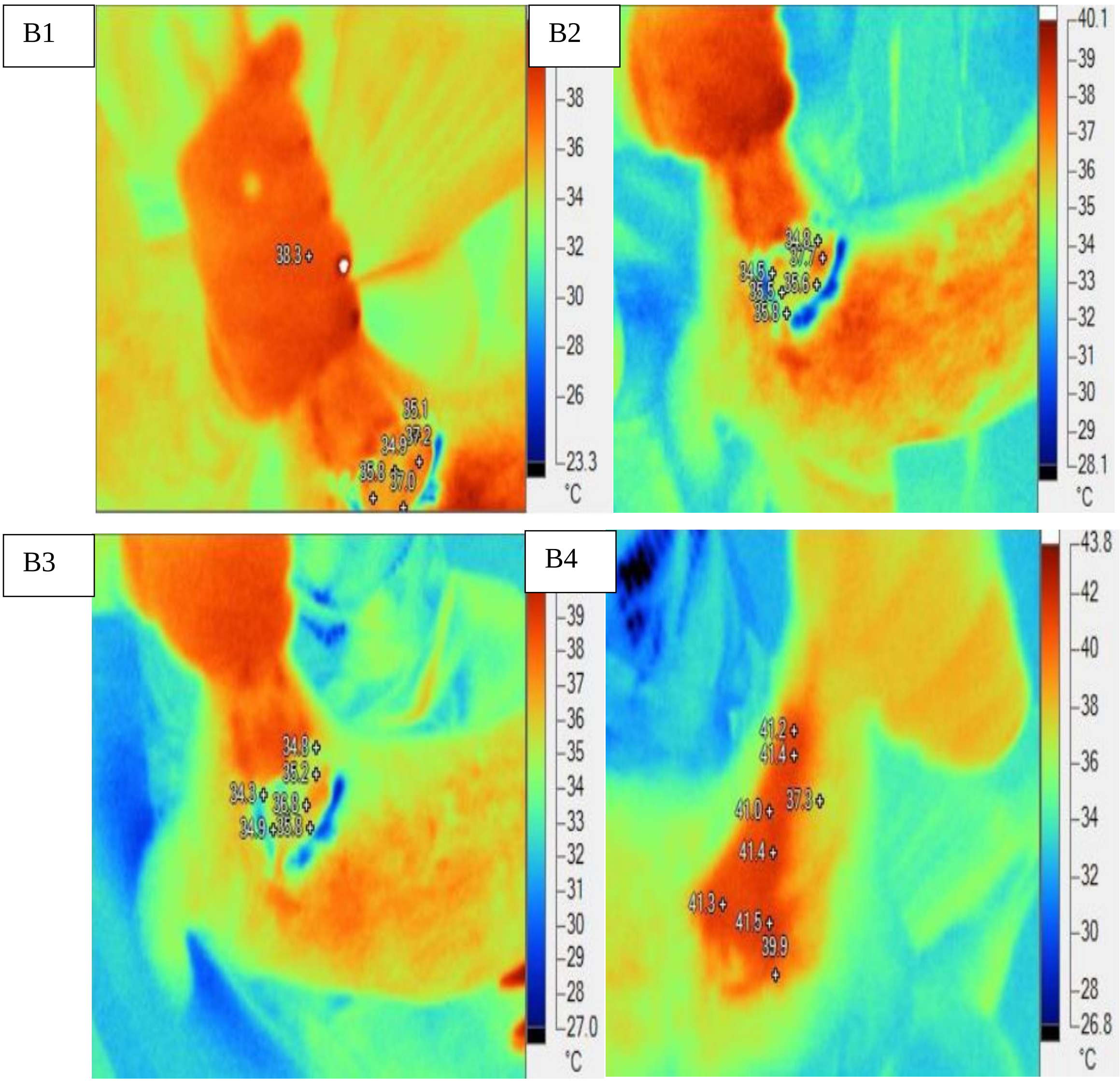

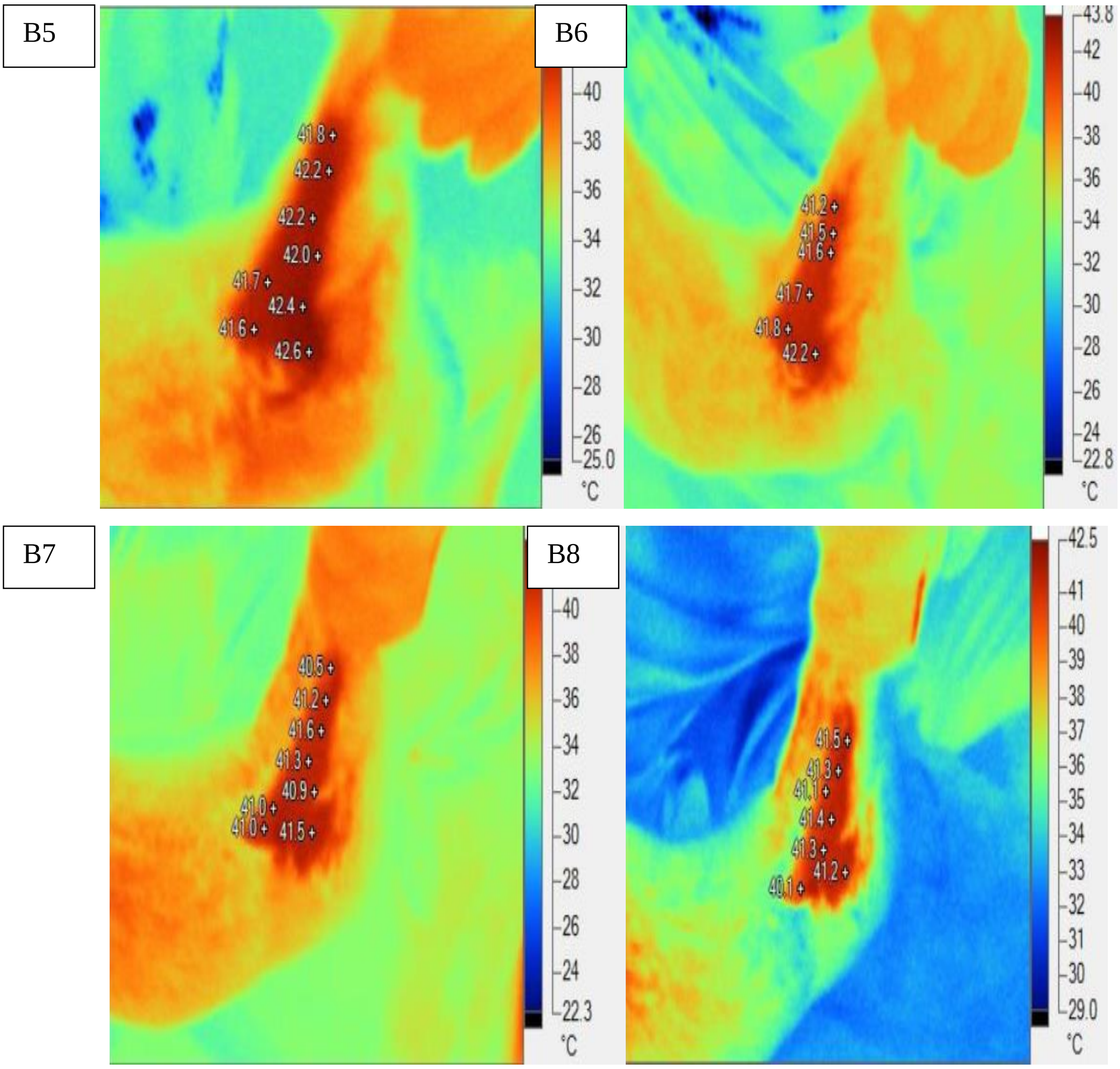

Figure (8): Original photos taken with radiation for rabbit skin, (B1, B2, B3) mix ZnO/Ag NPs with water,(B4, B5,B6,B7,B8) mix ZnO/Ag NPs with Vaseline.

Tables 1, 2, 3, and 4 provided an illustration of the end outcome. For picture R8 without radiation, the highest value in the range (3-5) µm was (0.9733), while for image R2* with radiation, the highest value in the range (8–12) µm was (0.9365).

Table (1) : The radiance for each image in the band (3-5)µm ,without irradiation

R1 T=33.9 -36.5 °c	R2 T=39.8 -45.9 °c	R3 T=41.4-42.8 °c	R4 T=39.4-43.5 °c	R5 T=38.8 - 43.5 °c	R6 T=51.3 - 53.5 °c	R7 T=52.1 - 54.1 °c	R8 T=53.1 - 54.9 °c	R9 T=50.6 - 55.4 °c	R10 T=53.4 - 55.3 °c
0.0010	0.0000	0.0418	0.0001	0.0000	0.0253	0.0594	0.1669	0.0012	0.0226
0.0019	0.0001	0.0527	0.0003	0.0001	0.0321	0.0733	0.2001	0.0020	0.0273
0.0035	0.0002	0.0664	0.0006	0.0002	0.0406	0.0902	0.2397	0.0033	0.0329
0.0065	0.0006	0.0835	0.0011	0.0005	0.0513	0.1109	0.2868	0.0056	0.0397
0.0121	0.0016	0.1049	0.0023	0.0012	0.0646	0.1362	0.3427	0.0092	0.0478
0.0221	0.0043	0.1316	0.0045	0.0027	0.0813	0.1669	0.4090	0.0151	0.0575
0.0400	0.0110	0.1648	0.0089	0.0060	0.1022	0.2042	0.4876	0.0245	0.0690
0.0719	0.0273	0.2060	0.0173	0.0129	0.1281	0.2495	0.5805	0.0393	0.0828
0.1282	0.0661	0.2572	0.0331	0.0274	0.1602	0.3044	0.6904	0.0627	0.0992
0.2266	0.1564	0.3206	0.0625	0.0570	0.2001	0.3708	0.8202	0.0992	0.1187
0.3972	0.3617	0.3991	0.1168	0.1168	0.2495	0.4510	0.9733	0.1557	0.1418

Table (2) : The radiance for each image in the band (8-14)µm,without irradiation

R1 T=33.9 -36.5 °c	R 2 T=39.8 -45.9 °c	R 3 T=41.4- 42.8 °c	R4 T=39.4- 43.5 °c	R5 T=38.8 - 43.5 °c	R6 T=51.3 - 53.5 °c	R7 T=52.1 - 54.1 °c	R8 T=53.1 - 54.9 °c	R9 T=50.6 - 55.4 °c	R10 T=53.4 - 55.3 °c
0.0272	0.0050	0.1573	0.0366	0.0229	0.0403	0.0576	0.0886	0.0293	0.1004
0.0356	0.0078	0.1733	0.0499	0.0331	0.0445	0.0629	0.0955	0.0365	0.1087
0.0463	0.0121	0.1908	0.0677	0.0473	0.0491	0.0685	0.1030	0.0453	0.1176
0.0599	0.0184	0.2099	0.0912	0.0672	0.0542	0.0747	0.1110	0.0561	0.1271
0.0774	0.0279	0.2308	0.1222	0.0946	0.0597	0.0814	0.1195	0.0691	0.1373
0.0995	0.0416	0.2536	0.1628	0.1321	0.0656	0.0886	0.1287	0.0849	0.1483
0.1275	0.0614	0.2786	0.2157	0.1831	0.0722	0.0963	0.1384	0.1038	0.1600
0.1628	0.0897	0.3057	0.2842	0.2519	0.0793	0.1047	0.1489	0.1266	0.1726
0.2071	0.1297	0.3353	0.3724	0.3443	0.0871	0.1138	0.1600	0.1537	0.1861
0.2626	0.1857	0.3676	0.4856	0.4672	0.0955	0.1235	0.1719	0.1861	0.2005
0.3318	0.2633	0.4027	0.6299	0.6299	0.1047	0.1340	0.1846	0.2245	0.2160

Table (3) : The radiance for each image in the band (3-5)µm

R1* T=34.9 -37.2°c	R2* T=34.8 -37.7 °c	R3* T=34.3 - 36.8 °c	R4* T=39.9- 41.5 °c	R5* T=41.6 - 42.6 °c	R6* T=41.2 - 42.2 °c	R7* T=40.5 - 41.6 °c	R8* T=40.1 - 41.5 °c
0.0011	0.0009	0.0026	0.0312	0.0582	0.0299	0.0902	0.0446
0.0019	0.0017	0.0048	0.0416	0.0686	0.0354	0.1092	0.0572
0.0032	0.0033	0.0087	0.0552	0.0809	0.0418	0.1320	0.0732
0.0054	0.0064	0.0156	0.0732	0.0952	0.0493	0.1595	0.0934
0.0090	0.0123	0.0278	0.0967	0.1120	0.0582	0.1925	0.1191
0.0150	0.0232	0.0491	0.1276	0.1316	0.0686	0.2321	0.1515
0.0247	0.0433	0.0860	0.1679	0.1545	0.0809	0.2795	0.1925
0.0406	0.0801	0.1496	0.2205	0.1813	0.0952	0.3363	0.2442
0.0662	0.1468	0.2581	0.2891	0.2126	0.1120	0.4042	0.3092
0.1074	0.2665	0.4421	0.3781	0.2492	0.1316	0.4853	0.3909
0.1732	0.4794	0.7517	0.4934	0.2917	0.1545	0.5822	0.4934

Table (4) : The radiance for each image in the band (8-14)µm

R1* T=34.9 -37.2°c	R2* T=34.8 -37.7 °c	R3* T=34.3 -36.8 °c	R4* T=39.9- 41.5 °c	R5* T=41.6 - 42.6 °c	R6* T=41.2 -42.2 °c	R7* T=40.5 -41.6 °c	R8* T=40.1 - 41.5 °c
0.0744	0.0675	0.0410	0.0534	0.1806	0.1368	0.0830	0.0619
0.0930	0.0895	0.0527	0.0601	0.1934	0.1467	0.0899	0.0687
0.1160	0.1182	0.0675	0.0677	0.2071	0.1573	0.0973	0.0761
0.1441	0.1554	0.0861	0.0761	0.2216	0.1686	0.1053	0.0842
0.1787	0.2033	0.1095	0.0855	0.2371	0.1806	0.1139	0.0932
0.2208	0.2650	0.1388	0.0959	0.2536	0.1934	0.1231	0.1031
0.2722	0.3438	0.1754	0.1076	0.2712	0.2071	0.1330	0.1139
0.3347	0.4443	0.2208	0.1205	0.2899	0.2216	0.1437	0.1257
0.4105	0.5719	0.2772	0.1349	0.3098	0.2371	0.1551	0.1387
0.5021	0.7332	0.3469	0.1508	0.3309	0.2536	0.1674	0.1530
0.6127	0.9365	0.4328	0.1686	0.3534	0.2712	0.1806	0.1686

The fur on the rabbit's skin was taken off. After that, the sample was applied to the skin in two different ways: first, by mixing it with water, as shown in figure 7: D1, D2, D3, D4, D5, and second, by using Vaseline, as shown in figure 7: D6, D7, D8, D9, and D10. The temperatures increased in both of the non-irradiation approaches.

(See Figure 8) for the identical material placement procedure. After the material was applied to the skin, it was heated to a temperature of 2 cm using a nozzle that was 75 cm away from the skin. Images were taken every two minutes during this process. In both situations, high temperatures were noted.

Using the Planck equation (2) in the tables (1, 2, 3, 4) and accounting for the camera's range, the radiation for each image was computed using the temperature change in the two bands (3-5)(8-14) µm.

The relationship between the radiance and temperature can be found by plotting them the output is shown in figure (9).

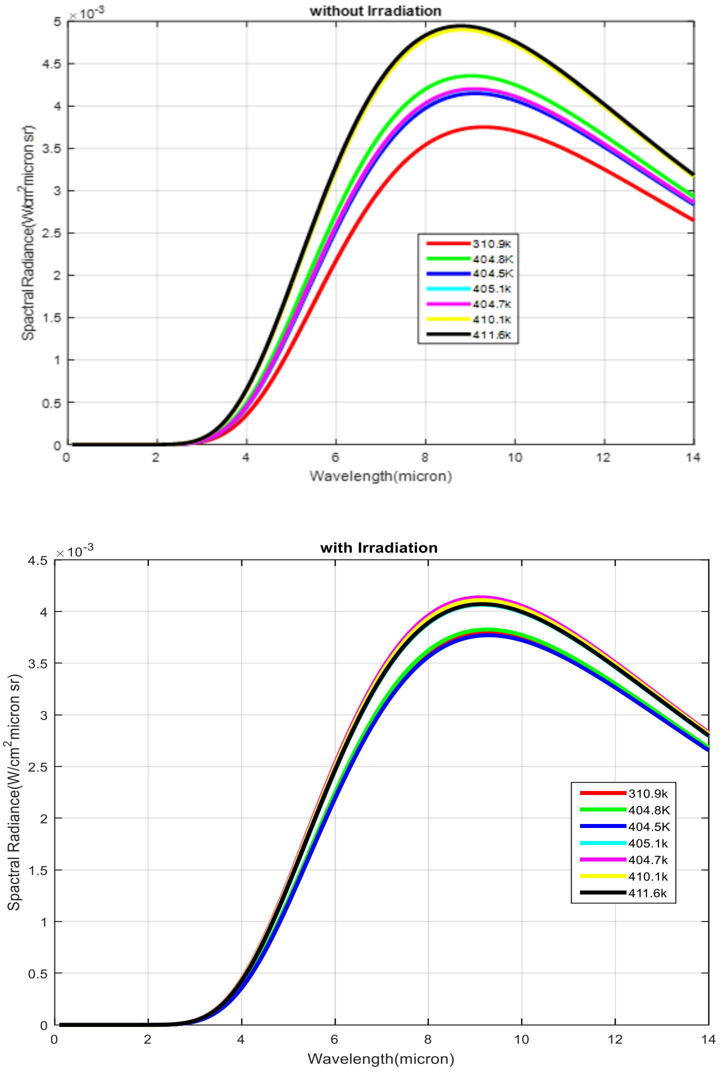

Fig.9. Spectral radiation emission at different temperatures (a) with irradiation, (b) without irradiation.

As the temperature rises, the total radiative emission, which is proportional to the area under the curve, grows quickly. As temperature rises, the maximum spectral radiation's wavelength moves towards shorter wavelengths. At all wavelengths, more spectral radiation is released at greater temperatures. Radial heat diffusion is found when data from line profiles at different temperatures are compared, as illustrated in Figure (9), which results in energy being transferred from the immersed NPs to the surrounding areas.

4. Conclusion

ZnO/Ag NPs with an estimated crystal size of 17.8 to 73.6 nm were successfully synthesised utilising a green synthesis process. When the ZnO/Ag NPs were sized and shaped by FE-SEM, they were found to have spherical, regular, and homogenous structures. The excitonic absorption peaks redshifted from 300 nm to 400 nm as a result of the UV absorption. The temperature was measured using thermal imaging equipment. Every image's radiation was computed based on temperature variations. The temperature grew together with the emission of light. As temperature rises, the maximum spectral radiation's wavelength moves towards shorter wavelengths. At all wavelengths, more spectral radiation is released at greater temperatures. Radial heat diffusion is seen when line profile data from various temperatures are compared, which results in energy being transferred from the submerged NPs to the surrounding areas.

Acknowledgment

Thanks and appreciation to the spray laboratory in the College of Science, Al-Mustansiriya University, Baghdad. And for the Ministry of Science and Technology in Baghdad.

References

1. M.R. Hashemzadeh et al. Stem cell therapy in the heart: biomaterials as a key route. Tissue Cell (2021).
2. T.M. Dawoud et al. Silver nanoparticles synthesized by Nigrospora oryzae showed antifungal activity ,Saudi J. Biol. Sci. (2021)
3. M.F. Zayed et al. In-vitro antioxidant and antimicrobial activities of metal nanoparticles biosynthesized using optimized Pimpinella anisum extract Colloids Surf. A Physicochem. Eng. Asp. (2020)
4. Z. Noohpisheh et al. Green synthesis of Ag-ZnO nanocomposites using Trigonella foenum-graecum leaf extract and their antibacterial, antifungal, antioxidant and photocatalytic properties Spectrochim. Acta Mol. Biomol. Spectrosc. (2020)
5. Z.F. Ma et al. Evaluation of phytochemical and medicinal properties of Moringa (Moringa oleifera) as a potential functional food South Afr. J. Bot. (2020)
6. S.M. Mousavi-Kouhi et al. Silver-zinc oxide nanocomposite: from synthesis to antimicrobial and anticancer properties Ceram. Int. (2021)
7. P.C. Nagajyothi et al. In vitro anticancer activity of eco-friendly synthesized ZnO/Ag nanocomposites Ceram. Int. (2021)
8. T.C. Prathna et al. Biomimetic synthesis of silver nanoparticles by Citrus limon (lemon) aqueous extract and theoretical prediction of particle size Colloids Surf. B Biointerfaces (2011)
9. H. Arslanoglu et al. Preparation of cation exchanger from lemon and sorption of divalent heavy metals. Bioresour. Technol. (2008)
10. T. Gur et al. Green synthesis, characterization and bioactivity of biogenic zinc oxide nanoparticles. Environ. Res. (2022)
11. M. Ashna et al. Greener synthesis of cerium oxide nanoemulsion using pollen grains of Brassica napus and evaluation of its antitumour and cytotoxicity properties Mater. Technol. (2020)
12. M.S. Amiri et al. Plant-based gums and mucilages applications in pharmacology and nanomedicine: a review Molecules (2021)

13. V.S. Sivasankarapillai et al. On facing the SARS-CoV-2 (COVID-19) with combination of nanomaterials and medicine: possible strategies and first challenges Nanomaterials (2020)
14. A. Es-haghi et al. Application of response surface methodology for optimizing the therapeutic activity of ZnO nanoparticles biosynthesized from Aspergillus Niger Biomimetics (2021)
15. M.E.T. Yazdi et al. Ultrasound-based synthesis of ZnO· Ag 2 O 3 nanocomposite: characterization and evaluation of its antimicrobial and anticancer properties Res. Chem. Intermed. (2021)
16. M.E. Taghavizadeh Yazdi et al. Biosynthesis, characterization, and antibacterial activity of silver nanoparticles using Rheum turkestanicum shoots extract Res. Chem. Intermed. (2018)
17. A.M. Pillai et al. Green synthesis and characterization of zinc oxide nanoparticles with antibacterial and antifungal activity J. Mol. Struct. (2020)
18. P.S. Ng et al. Citrullus lanatus mediated-green synthesis of Ag/ZnO composite for photocatalytic degradation of 2, 4-dichlorophenoxyacetic acid
19. M.R. Shaik et al. Plant-extract-assisted green synthesis of silver nanoparticles using Origanum vulgare L. extract and their microbicidal activities Sustainability (2018)
20. Visible light driven Ni doped hematite for photocatalytic reduction of noxious methylene blue 2023, Materials Research Bulletin
21. Photocatalytic Degradation, Anticancer, and Antibacterial Studies of Lysinibacillus sphaericus Biosynthesized Hybrid Metal/Semiconductor Nanocomposites 2023, Microorganisms
22. Green synthesis of silver nanoparticles and its potential applications 2023, Applications of Silver Nanoparticles.
23. Abdul Samad , F. , Peng, Z. , Yongfeng , G. , Raza , G., Emerging radiative materials and prospective applications of radiative sky cooling. Renewable and Sustainable Energy Reviews. (2012).
24. P. Mahajan, A. Singh, S. Arya, Improved performance of solution processed organic solar cells with an additive layer of sol-gel synthesized ZnO/CuO core/shell nanoparticles, J Alloys Compd 814 (2020) 152292, https://doi.org/10.1016/ j.jallcom.2019.152292.
25. A. Singh, A. Ahmed, A. Sharma, C. Sharma, S. Paul, A. Khosla, V. Gupta, S. Arya, Promising photocatalytic degradation of methyl orange dye via sol-gel synthesized AgeCdS@Pr-TiO2 core/shell nanoparticles, Phys B Condens Matter 616 (2021) 413121, https://doi.org/10.1016/j.physb.2021.413121.